Journal of Biomedical Optics

BiomedicalOptics.SPIEDigitalLibrary.org

Photoacoustic thermal flowmetry with a single light source

Wei Liu
Bangxin Lan
Leo Hu
Ruimin Chen
Qifa Zhou
Junjie Yao

SPIE.

Wei Liu, Bangxin Lan, Leo Hu, Ruimin Chen, Qifa Zhou, Junjie Yao, "Photoacoustic thermal flowmetry with a single light source," *J. Biomed. Opt.* **22**(9), 096001 (2017), doi: 10.1117/1.JBO.22.9.096001.

Journal of Biomedical Optics 22(9), 096001 (September 2017)

Photoacoustic thermal flowmetry with a single light source

Wei Liu,[a] Bangxin Lan,[a] Leo Hu,[a] Ruimin Chen,[b] Qifa Zhou,[b] and Junjie Yao[a,*]
[a]Duke University, Department of Biomedical Engineering, Durham, North Carolina, United States
[b]University of Southern California, Department of Biomedical Engineering, Los Angeles, California, United States

Abstract. We report a photoacoustic thermal flowmetry based on optical-resolution photoacoustic microscopy (OR-PAM) using a single laser source for both thermal tagging and photoacoustic excitation. When an optically absorbing medium is flowing across the optical focal zone of OR-PAM, a small volume of the medium within the optical focus is repeatedly illuminated and heated by a train of laser pulses with a high repetition rate. The average temperature of the heated volume at each laser pulse is indicated by the photoacoustic signal excited by the same laser pulse due to the well-established linear relationship between the Grueneisen coefficient and the local temperature. The thermal dynamics of the heated medium volume, which are closely related to the flow speed, can therefore be measured from the time course of the detected photoacoustic signals. Here, we have developed a lumped mathematical model to describe the time course of the photoacoustic signals as a function of the medium's flow speed. We conclude that the rising time constant of the photoacoustic signals is linearly dependent on the flow speed. Thus, the flow speed can be quantified by fitting the measured photoacoustic signals using the derived mathematical model. We first performed proof-of-concept experiments using defibrinated bovine blood flowing in a plastic tube. The experiment results have demonstrated that the proposed method has high accuracy ($\sim \pm 6\%$) and a wide range of measurable flow speeds. We further validated the method by measuring the blood flow speeds of the microvasculature in a mouse ear *in vivo*. [DOI: 10.1117/1.JBO.22.9.096001]

Keywords: photoacoustic imaging; optical-resolution photoacoustic microscopy; thermal flowmetry; thermal tagging; blood flow.

Paper 170433LR received Jul. 6, 2017; accepted for publication Aug. 9, 2017; published online Sep. 5, 2017.

1 Introduction

Blood flow speed is an important functional parameter of the biological tissue.[1] Accurately measuring blood flow speed is critical for diagnosing many diseases, such as burns,[2] stroke,[3] and atherosclerosis.[4] Presently, photoacoustic tomography,[5–7] which combines optical excitation and acoustic detection, has attracted great attention for measuring blood flow speeds due to its excellent capability to detect blood using hemoglobin as the endogenous contrast.[8–21] So far, many photoacoustic methods have been reported for blood flow measurement, based on the Doppler effect,[9,19,20] thermal tagging,[10,12] and signal-fluctuation correlation.[13,17,18] Although the Doppler- and correlation-based methods have been successfully demonstrated *in vivo*, both methods depend on tracking varying photoacoustic signal signatures, which requires the absorbers to be distributed with sufficient spatial heterogeneity. By contrast, the thermal-tagging-based methods can be applied to both homogenous and inhomogeneous flowing media. Sheinfeld and Eyal[10] pioneered the photoacoustic thermal-tagging flowmetry by investigating the dependence of the photoacoustic signals on temperatures and flow speeds, using two lasers as the thermal-tagging and photoacoustic excitations, respectively. Later, this method was improved by Wang et al.[12] by employing a focused high-intensity-focused ultrasound (HIFU) transducer as the thermal-tagging source on acoustic-resolution photoacoustic microscopy (AR-PAM). The blood flow at depths of several millimeters can be measured, taking advantage of the deep-penetration of the HIFU heating. However, this method was not readily applicable for *in vivo* blood flow measurement, since the HIFU heating and photoacoustic detection are placed at the opposite sides of the sample. Furthermore, only the cooling process can be monitored because of the acoustic interference between the HIFU transducer and the photoacoustic detection. Zhang et al.[22] further expanded the thermal-tagging method using optical-resolution photoacoustic microscopy (OR-PAM) and two independent light sources for thermal-tagging and photoacoustic excitation, which have limited its applications in traditional OR-PAM systems where only a single light source is typically available.

To address the above issues, we present a thermal-tagging-based photoacoustic flowmetry using OR-PAM with only a single light source. Compared with AR-PAM, OR-PAM can provide higher spatial resolutions, and thus a better thermal-tagging efficiency, at the cost of penetration depth.[16] In addition, because OR-PAM has higher light-usage efficiency and uses less laser energy, a high pulse repetition rate can be explored for measuring fast blood flow speeds. In this work, instead of diffused optical heating[10] or focused ultrasound heating,[12] we use a focused laser beam with a short pulse width and a high repetition rate for both thermal tagging and photoacoustic excitation. Such a simplified configuration enables reflection-mode thermal tagging and photoacoustic imaging using the same light source, which is highly desired for *in vivo* blood flow measurements. In addition, we have developed the mathematical model to describe the thermal-tagging process and a practical fitting

*Address all correspondence to: Junjie Yao, E-mail: junjie.yao@duke.edu

1083-3668/2017/$25.00

method to quantify the flow speeds based on the measured temperature-dependent photoacoustic signals. In the following sections, we will present the mathematical model together with proof-of-concept experiments and further validate it via *in vivo* blood flow measurements.

2 Theory and Method

The principle of photoacoustic thermal flowmetry originates from the well-established dependence of photoacoustic signal amplitude on the temperature of the flowing medium, which can be modulated by external heating and affected by the flow speed.[23,24]

2.1 *Local Temperature Change by Laser Heating*

To quantify the flow speed using the temperature-dependent photoacoustic signals in OR-PAM, the relationship between the local medium temperature and its flow speed must first be modeled. As the train of focused laser pulses heats the medium, the local temperature within the heated volume increases from its baseline temperature before the heating. Note that the thermal diffusion in the heated volume may not be negligible in our model, meaning that the heated volume may be larger than the optical focus, depending on the total heating time. The temperature T can be modeled as[10]

$$\frac{\partial T(\vec{r},t)}{\partial t} = \nabla[\alpha(\vec{r})\nabla T(\vec{r},t)] - v(\vec{r})\nabla T(\vec{r},t) + s(\vec{r}), \tag{1}$$

where $\vec{r}$ is the spatial coordinate in the heated volume, t is the time, ∇ is the differential operator in three-dimensional Cartesian coordinates, $\alpha(\vec{r})$ is the thermal diffusivity, $v(\vec{r})$ is the flow speed, and $s(\vec{r})$ is the thermal flux density provided by the focused laser pulses. The left side of Eq. (1) denotes the rate of temperature change due to the three contributions on the right side of Eq. (1): the thermal conduction, thermal convection, and heating source. While the thermal conduction is mainly due to the random Brownian motion, the thermal convection is dominated by the coherent flow of the medium. The initial condition for solving Eq. (1) is given by

$$T(\vec{r},t) = T(\vec{r},t_0), \tag{2}$$

where t_0 is the time point when laser heating starts.

Equation (1) is further simplified using a lumped model.[12] Both sides of Eq. (1) are weight-averaged within the heated volume by introducing a weighted spatial integration as

$$\frac{\partial}{\partial t}\left[\oint_\Omega \omega_1(\vec{r})T(\vec{r},t)\mathrm{d}V\right] = \oint_\Omega \omega_1(\vec{r})\{\nabla[\alpha(\vec{r})\nabla T(\vec{r},t)] - v(\vec{r})\nabla T(\vec{r},t) + s(\vec{r})\}\mathrm{d}V, \tag{3}$$

where Ω is the heated volume and $\omega_1(\vec{r})$ is the weight function of the lumped model. $\omega_1(\vec{r})$ is unknown. If the average temperature within the heated volume is defined as

$$\overline{T(t)} = \oint_\Omega \omega_1(\vec{r})T(\vec{r},t)\mathrm{d}V, \tag{4}$$

then Eq. (3) can be simplified as

$$\frac{\partial \overline{T(t)}}{\partial t} = \oint_\Omega \omega_1(\vec{r})\left\{\nabla\left[\alpha(\vec{r})\nabla\frac{T(\vec{r},t)}{\overline{T(t)}}\right] - v(\vec{r})\nabla\frac{T(\vec{r},t)}{\overline{T(t)}}\right\}\overline{T(t)}\mathrm{d}V + \oint_\Omega \omega_1(\vec{r})s(\vec{r})\mathrm{d}V, \tag{5}$$

For a stable flow, we can assume that $T(\vec{r},t)/\overline{T(t)}$ is time-invariant. This assumption means that the relative temperature distribution within the heated volume does not change with time. In other words, the relative spatial contribution of each part of the heated volume is time-invariant. This assumption is more accurate for a small heated volume.[12] Equation (5) can then be rewritten as

$$\frac{\partial \overline{T(t)}}{\partial t} = -(C_\alpha + C_v)\overline{T(t)} + C_s, \tag{6}$$

where the three coefficients of the right side of Eq. (6) are expressed as

$$C_\alpha = \oint_\Omega \omega_1(\vec{r})\nabla\left[\alpha(\vec{r})\nabla\frac{T(\vec{r},t)}{\overline{T(t)}}\right]\mathrm{d}V, \tag{7}$$

$$C_v = -\oint_\Omega \omega_1(\vec{r})v(\vec{r})\nabla\frac{T(\vec{r},t)}{\overline{T(t)}}\mathrm{d}V, \tag{8}$$

$$C_s = \oint_\Omega \omega_1(\vec{r})s(\vec{r})\mathrm{d}V. \tag{9}$$

After solving Eq. (6), which is a first-order differential equation, the average temperature within the heated volume can be obtained as

$$\overline{T(t)} = e^{-(C_\alpha+C_v)t}\left[\overline{T(t_0)} - \frac{C_s}{C_\alpha+C_v}\right] + \frac{C_s}{C_\alpha+C_v}, \tag{10}$$

where $\overline{T(t_0)}$ indicates the baseline of the local temperature. Here, the average local temperature as a function of heating time has been estimated, which is simply an exponential recovery function. Specifically, Eqs. (8) and (9) show that, given homogeneous distributions of $v(\vec{r})$ and $\alpha(\vec{r})$, the two coefficients C_v and C_α are proportional to the flow speed and thermal diffusivity, respectively. Again, the approximation of homogenous $v(\vec{r})$ and $\alpha(\vec{r})$ is more accurate for flow measurements in small blood vessels or optical wavelengths with shallow penetration into blood vessels. Then, we can define a compound thermal constant C as

$$C = C_\alpha + C_v = k_1\alpha + k_2 v, \tag{11}$$

where k_1 and k_2 themselves are two compound constant factors. In this case, Eq. (10) is finally simplified as

$$\overline{T(t)} = e^{-Ct}\left[\overline{T(t_0)} - \frac{C_s}{C}\right] + \frac{C_s}{C}. \tag{12}$$

2.2 *Photoacoustic Sensing of the Local Temperature*

The next step is to establish how the local temperature can be sensed by photoacoustic signals. In our method, the laser pulse

width is short enough to satisfy both the thermal and stress confinements, thus the initial photoacoustic pressure rise is given by[25]

$$P(\vec{r},t)=\Gamma(\vec{r},t)\eta(\vec{r})\mu_a(\vec{r})F(\vec{r}), \tag{13}$$

where $\mu_a(\vec{r})$ is the optical absorption coefficient (cm^{-1}), $F(\vec{r})$ is the local optical fluence ($\mathrm{mJ/cm}^2$), $\eta_{\mathrm{th}}(\vec{r})$ is the percentage that the absorbed photon energy is converted into thermal energy, and $\Gamma(\vec{r},t)$ is the Grüeneisen parameter, which is a temperature-dependent parameter that determines the conversion efficiency of thermal energy to the acoustic energy. For diluted aqueous solutions, $\Gamma(\vec{r},t)$ has a linear relationship with the baseline temperature T and can be represented by the following empirical formula as

$$\Gamma(\vec{r},t)=a+bT(\vec{r},t), \tag{14}$$

where a and b are two positive constants.

Substituting Eq. (14) into Eq. (13), we obtain

$$P(\vec{r},t)=a\eta_{\mathrm{th}}(\vec{r})\mu_a(\vec{r})F(\vec{r})+bT(\vec{r},t)\eta_{th}(\vec{r})\mu_a(\vec{r})F(\vec{r}). \tag{15}$$

Following the same approach of obtaining the spatial-weighted average temperature within the heated volume, the spatial-weighted average pressure amplitude is obtained by introducing the second weight spatial integration as

$$\begin{aligned}\overline{P(t)}&=\oint_\Omega \omega_2(\vec{r})P(\vec{r},t)\mathrm{d}V\\&=a\oint_\Omega \omega_2(\vec{r})\eta_{th}(\vec{r})\mu_a(\vec{r})F(\vec{r})\mathrm{d}V\\&\quad+b\overline{T(t)}\oint_\Omega \omega_2(\vec{r})\eta_{th}(\vec{r})\mu_a(\vec{r})F(\vec{r})\frac{T(\vec{r},t)}{\overline{T(t)}}\mathrm{d}V,\end{aligned} \tag{16}$$

where $\omega_2(\vec{r})$ is the second weight function for the initial pressure rise. For simplicity, the time-invariant terms of the right side of Eq. (16) are defined as

$$C_1=a\oint_\Omega \omega_2(\vec{r})\eta_{\mathrm{th}}(\vec{r})\mu_a(\vec{r})F(\vec{r})\mathrm{d}V, \tag{17}$$

$$C_2=b\oint_\Omega \omega_2(\vec{r})\eta_{\mathrm{th}}(\vec{r})\mu_a(\vec{r})F(\vec{r})\frac{T(\vec{r},t)}{\overline{T(t)}}\mathrm{d}V, \tag{18}$$

which are also two constant factors. Then, Eq. (16) can be rewritten as

$$\overline{P(t)}=C_1+C_2\overline{T(t)}. \tag{19}$$

Substituting Eq. (12) into Eq. (19), the initial average photoacoustic pressure is given by

$$\overline{P(t)}=e^{-Ct}\left[C_2\overline{T(t_0)}-\frac{C_sC_2}{C}\right]+C_1+\frac{C_2C_s}{C}, \tag{20}$$

which appears as a derivative form of an exponential function. Therefore, the thermal constant C can be obtained by simply fitting the measured photoacoustic signals amplitudes as function of the heating time as

$$\overline{P(t)}=Ae^{-Ct}+B, \tag{21}$$

where A and B are the two constant factors that have a complex relationship with the spatial resolution of the imaging system, the absorption coefficient of the flowing medium, and the power of the heating source. By contrast, the thermal constant C has a relatively simple linear relationship with the flow speed v [see Eq. (11)] if the thermal diffusivity α is a constant. With the knowledge of C fitted from the measured photoacoustic signals, the flow speed v can be estimated if the slope k_2 and the intercept $k_1\alpha$ can be calibrated.

At the end of this section, the maximum measurable flow speed of the proposed method is estimated here. Assuming that at least two measurements (or laser pulses) are required for accurate fitting of the thermal constant C, then the total flow distance d during two laser pulses is calculated by

$$d=v_{\max}\frac{1}{f}, \tag{22}$$

where f is the laser repetition rate. Theoretically, d should be shorter than the maximum transverse length of the heated volume. For the first-order approximation, the maximum transverse length L is estimated as the optical focal zone

$$L=0.87\lambda/\mathrm{NA}, \tag{23}$$

where NA denotes the numerical aperture of the focusing lens. Hence, we have

$$d\le L\Rightarrow v_{\max}\le 0.87\lambda f/\mathrm{NA}. \tag{24}$$

As a result, the maximum measurable flow speed can be improved by increasing the laser repetition rate or enlarging the heating zone. Note that the number of measurements needed majorly depends on the signal-to-noise ratio of the imaging system and the measured flow speeds.

2.3 *Optical-Resolution Photoacoustic Thermal Flowmetry*

The schematic of a reflection-mode OR-PAM system is shown in Fig. 1(a). The pulse-laser beam from an Nd:YAD laser (IS8II-E, Edgewave, Würselen, Germany), with a wavelength of 532 nm and a pulse width of 5 ns, was expanded by two convex lenses and then focused by a focusing lens with a focal length of 50 mm (AC127-050-A, Thorlabs, Newton, New Jersey). Defibrinated bovine blood (Quad Five, Ryegate, Montana) was flowed in a transparent plastic tube (inner diameter: 0.3 mm, Dow Corning, Cat. 508-001, Midland, Michigan) driven by a syringe pump (NE-1000, New Era, Farmingdale, New York). The blood flow speeds were precisely controlled by adjusting the syringe pump's translation speeds. The flowing blood was then thermally tagged and photoacoustically excited by a train of laser pulses. The laser pulse energy was 37 nJ, and the light was focused about 50 μm below the sample surface. The optical fluence at the sample surface was ~37 $\mathrm{mJ/cm}^2$, which is slightly higher than the ANSI limit (20 $\mathrm{mJ/cm}^2$) but below the damage threshold.[26] A photodiode (DET025A, Thorlabs, Newton, New Jersey) sampled a small portion of the laser pulse to measure the energy of each laser pulse. A function generator (DG1022, Beaverton, Oregon) was used to generate 50 kHz trigger signals to synchronize the laser firing and

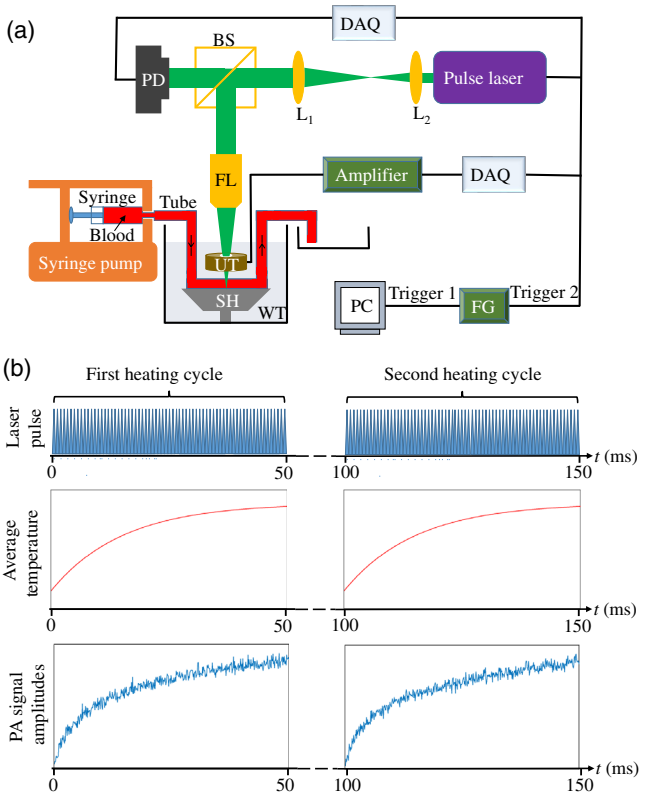

Fig. 1 Optical-resolution photoacoustic thermal flowmetry. (a) Schematics of the setup. BS, beam sampler; DAQ, data acquisition; FG, function generator; FL, focusing lens; L_1 and L_2, convex lens; PC, personal computer; PD, photodiode; SH, sample holder; WT, water tank; UT, ultrasonic transducer. (b) Schematics of the time courses of the laser pulses, the average local temperature, and the average photoacoustic signal amplitudes during each heating cycle.

data acquisition (DAQ). A focused ring ultrasonic transducer (central frequency: 30 MHz, bandwidth: 30 MHz) detected the photoacoustic signal amplitudes of the heated region. The photoacoustic signals were amplified by 51 dB and sampled at 500 MHz. The lateral resolution of the system is ~5 μm, and the axial resolution is ~42 μm.

Peak-to-peak amplitudes of the photoacoustic signals were extracted as a function of heating time (or number of laser pulses). We used 500 laser pulses at 10 kHz for each heating cycle that had a duration of 50 ms. Each heating cycle was 100 ms apart from the next to ensure the heated blood had enough time to flow out of the heating zone before the start of the next heating cycle, as shown in Fig. 1(b). For each heating cycle, the average temperature within the heated volume was elevated from its baseline, resulting in an increase in the average photoacoustic signal amplitude within the same volume. We repeated the heating for 40 cycles to improve the measurement accuracy.

3 Results and Discussion

Calibration experiments were first performed with different flow speeds ranging from 0 to 54 mm/s in 6 mm/s increments. We monitored the laser pulse energy during each heating cycle using the photodiode readings, as shown in Fig. 2(a). A pulse energy fluctuation of 2.2% was observed, showing the relatively high stability of heating power. The photoacoustic signal amplitude

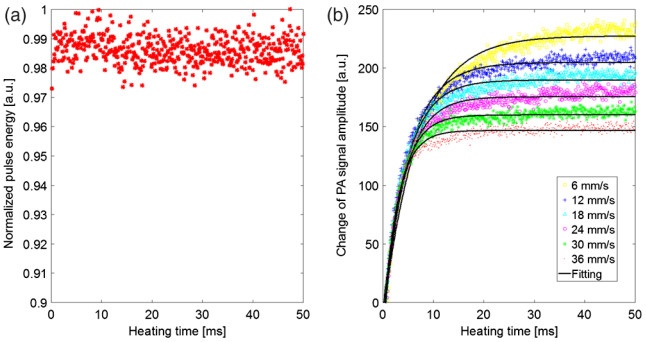

Fig. 2 Laser pulse energy and photoacoustic signal amplitudes as a function of heating time at different flow speeds obtained on bovine blood phantoms. (a) Normalized laser pulse energy versus heating time, showing a relatively stable heating power. (b) The change in photoacoustic signal amplitudes at different flow speeds, showing the different temperature rising times and equilibrium temperatures. The fitting curves were based on Eq. (21).

upon each laser pulse was acquired during each heating cycle. At each flow speed, 40 heating cycles were performed and the results were averaged. Figure 2(b) shows the averaged time courses of the change in photoacoustic signal amplitudes at six representative flow speeds ranging from 6 to 36 mm/s. The baseline photoacoustic signals obtained with the initial laser pulses were subtracted from all the signals. The results have shown that the measured photoacoustic signal amplitudes initially increased with the heating time before reaching equilibrium. A higher flow speed resulted in a shorter temperature rising time and a lower equilibrium temperature, which was consistent with Eq. (20). The equilibrium temperature was reached when the initial volume of the low-temperature blood had flowed out of the heating zone. Once the equilibrium was reached, the blood volume within the heating zone became thermally "stationary," even though blood was still flowing through. Data fitting was then performed on the measured photoacoustic signal amplitudes using Eq. (21). The fitting curves are shown as the black solid lines in Fig. 2(b), which correspond to the six different flow speeds. The thermal constants in Eq. (11) at all flow speeds can thus be obtained from the fittings.

As expected in Eq. (11), the thermal constant should be linearly dependent on the flow speed. This linear relationship can be readily validated by fitting the thermal constant as a function of the flow speed. To determine the slope k_2 and the intercept $k_1\alpha$, a total of 10 thermal constants were obtained at 10 different flow speeds, as shown in Fig. 3(a). The fitting has a coefficient of determination (R^2 value) of 0.99, showing a strong linear dependence of the thermal constant on flow speed, which is consistent with Eq. (11). k_2 and $k_1\alpha$ are fitted as 35.44 ± 2.34 and 511.74 ± 78.05, respectively. These two calibration values will be used for quantifying unknown flow speeds if we can assume the thermal diffusivity α (material-dependent) of the biological tissue is consistent. After the system was calibrated, we further measured 10 more different flow speeds based on the calibration values. Figure 3(b) shows the measured flow speeds agreed well with the true flow speeds ranging from 3 to 57 mm/s. The averaged measurement error was 6.2%. Here, it is necessary to point out that due to the relatively long heating time of 50 ms, the thermal diffusion in the flowing medium cannot be neglected. Therefore, the heating zone was effectively much larger than the optical focal zone. Increasing the laser repetition rate will effectively shorten the effective heating zone.

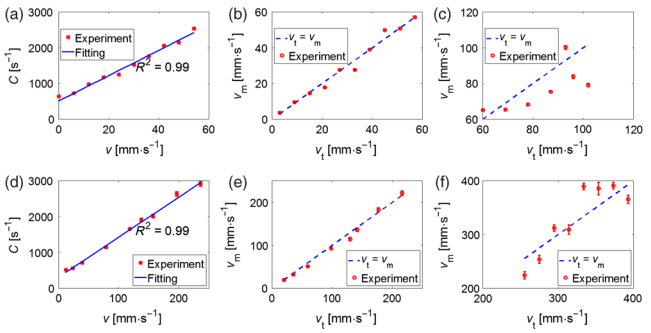

Fig. 3 Optical-resolution photoacoustic thermal flowmetry on bovine blood phantoms. (a)–(c) were acquired with a laser repetition rate of 10 kHz, and (d)–(e) were acquired with a laser repetition rate of 50 kHz. (a, d) Thermal constant C as a function of flow speed v in the calibration experiment. (b, e) Measured flow speeds (v_m) versus the true flow speeds (v_t). (c, f) Measured flow speeds versus true flow speeds beyond the maximum measurable flow speed. Error bars are standard errors.

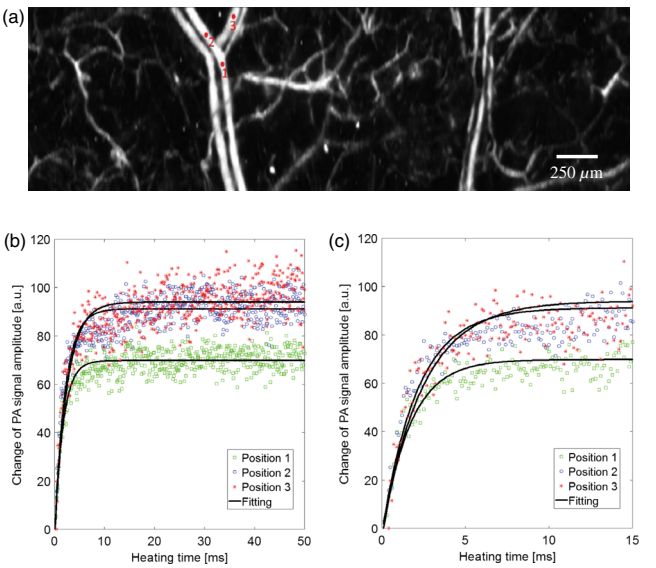

Fig. 4 *In vivo* blood flow measurements in a mouse ear. (a) Maximum amplitude projection image of the measured area. The three measured vessels are indicated by the solid red circles. (b) The changes in photoacoustic signal amplitudes in each heating cycle at the three vessels. Fittings are based on Eq. (21). (c) The more detailed changes in photoacoustic signal amplitudes from 0 to 15 ms.

Validation experiments for maximum measurable flow speeds were also performed at the flow speeds from 60 to 102 mm/s, as shown in Fig. 3(c). The results show an increased measurement error of more than 20%. The maximum measurable speed of the system can be improved by increasing the laser repetition rate. As a simple demonstration, we used another Nd:YAG laser (VPFL-G-20, V-gen, Tel Aviv, Israel) with a laser repetition rate of 50 kHz. Figures 3(d) and 3(e) show the results with the flow speeds ranged from 11.8 to 236 mm/s. The averaged measurement error is 6.3%. When the flow speed is beyond the maximum measurable speed, the increased measurement error is shown in Fig. 3(f). The effective optical NAs for the EdgeWave laser beam (10 kHz) and the V-gen laser beam (50 kHz) are 0.1 and 0.13, respectively. The maximum measurable flow speeds are 46.3 mm/s for the 10 kHz laser and 178.1 mm/s for the 50 kHz laser, according to Eq. (24). Additionally, because the fitting process is more robust when the local temperature reaches the equilibrium, a higher laser repetition rate also limits the ability to measure slow flows when the total number of pulses per heating cycle remains the same.

To further test the proposed flowmetry, *in vivo* measurements were performed by measuring the blood flow speeds of the microvasculature in a mouse ear. The *in vivo* study was conducted on a female Swiss Webster mouse (10 weeks old and 32.1 g in weight), with the protocol approved by the Institutional Animal Care and Use Committee of Duke University. The region of interest for the blood flow measurement was first imaged by the OR-PAM system, as shown in Fig. 4(a). The *in vivo* blood flow speed measurements were then performed with a 10 kHz laser pulse repetition rate. Like the phantom experiments, each heating cycle had 500 laser pulses and was repeated 40 times to improve the measurement accuracy. The laser pulse energy was 34 nJ. The three measurement positions on the mouse ear were indicated by the red solid circles in Fig. 4(a). The changes in photoacoustic signal amplitudes versus heating time were shown in Fig. 4(b), and the major changes at the beginning of the heating from 0 to 15 ms were shown in Fig. 4(c). The three thermal constants were fitted as 602.6, 545.7, and 546 s^{-1}, corresponding to respective blood flow speeds of 2.56, 0.96, and 0.99 mm/s, which generally agree with our previous study.[9] Note that point 1 and point 2 are at different branch levels of an artery, with point 1 on the mother branch and point 2 on the daughter branch. Hence, the flow speed at point 1 should be faster than point 2.

4 Conclusion

In conclusion, we have developed a new photoacoustic thermal flowmetry with a single light source, which can be readily applied on traditional reflection-mode OR-PAM systems. The same light source is used for simultaneous thermal tagging and photoacoustic imaging. We have developed a mathematic model to establish the relation between the flow speed and the thermal constant extracted from the detected photoacoustic signal amplitudes. We have performed calibration experiments to determine the system-dependent and medium-dependent constant factors. We have verified the new method on flowing blood phantoms at speeds up to 236 mm/s and validated its effectiveness for *in vivo* measurements by measuring the blood flow speeds of the microvasculature in a mouse ear.

Compared with the previous photoacoustic flowmetry,[9,10,12,13,17–21] the new method can be applied to both homogenous and inhomogeneous media and can measure relatively high flow speeds with high spatial resolutions. However, due to the limited penetration of OR-PAM, the new method is only applicable for quasiballistic regimes (~1 mm deep in the skin). To increase the penetration depth, we can apply near-infrared wavelength light[27,28] or wavefront-shaping technologies that can help focus the light into deep scattering tissues.[29,30] In addition, due to the symmetry of the heating (imaging) zone, the proposed method is not sensitive to the lateral flow direction. The lateral flow direction can be determined by scanning the flowing media with two opposite scanning directions, as we have demonstrated before.[9] Moreover, a high laser repetition rate on the level of hundreds of kilohertz is required for the high-speed flow measurements, such as blood flow in major arteries, to ensure a high measurement accuracy; for the slow-speed measurements, such as in microvasculature, a laser repetition rate of tens of kilohertz is needed. In addition, the focal

spot size of the light beam is important. A relatively large spot size is preferred for measuring the high-speed blood flows. Finally, the imaging time of the proposed method is a concern for 2-D flow mapping, especially for slow flows. We can potentially shorten the imaging time by increasing the laser repetition rate or decreasing the laser focal spot size, which can decrease the dwell time at each scanning position.

Disclosures

All authors have no financial interest.

Acknowledgments

We would like to thank the financial support by Duke MEDx fund to Junjie Yao.

References

1. Y. Jiang et al., "Blood oxygen flux estimation with a combined photoacoustic and high-frequency ultrasound microscopy system: a phantom study," *J. Biomed. Opt.* **17**(3), 036012 (2012).
2. F. E. Gump, J. B. Price, and J. M. Kinney, "Blood flow and oxygen consumption in patients with severe burns," *Surg. Gynecol. Obstet.* **130**(1), 23 (1970).
3. X. H. Zhu et al., "Simultaneous and noninvasive imaging of cerebral oxygen metabolic rate, blood flow and oxygen extraction fraction in stroke mice," *NeuroImage* **64**, 437–447 (2013).
4. M. Beraia and G. Beraia, "Investigation of the blood flow at the boundary layer by the magnetic resonance angiography in atherosclerosis," *Atherosclerosis* **235**(2), E156 (2014).
5. L. H. V. Wang and J. J. Yao, "A practical guide to photoacoustic tomography in the life sciences," *Nat. Methods* **13**(8), 627–638 (2016).
6. J. Weber, P. C. Beard, and S. E. Bohndiek, "Contrast agents for molecular photoacoustic imaging," *Nat. Methods* **13**(8), 639–650 (2016).
7. P. K. Upputuri and M. Pramanik, "Recent advances toward preclinical and clinical translation of photoacoustic tomography: a review," *J. Biomed. Opt.* **22**(4), 041006 (2017).
8. J. A. Viator et al., "Gold nanoparticle mediated detection of prostate cancer cells using photoacoustic flowmetry with optical reflectance," *J. Biomed. Nanotechnol.* **6**(2), 187–191 (2010).
9. J. J. Yao et al., "*In vivo* photoacoustic imaging of transverse blood flow by using Doppler broadening of bandwidth," *Opt. Lett.* **35**(9), 1419–1421 (2010).
10. A. Sheinfeld and A. Eyal, "Photoacoustic thermal diffusion flowmetry," *Biomed. Opt. Express* **3**(4), 800–813 (2012).
11. J. A. Viator, B. S. Goldschmidt, and K. D. Rood, "Detecting circulating melanoma cells in blood using photoacoustic flowmetry," in *Biosensors and Molecular Technologies for Cancer Diagnostics*, K. Herold and A. Rasooly, Eds., pp. 505–514, CRC Press, Boca Raton, Florida (2012).
12. L. D. Wang et al., "Ultrasound-heated photoacoustic flowmetry," *J. Biomed. Opt.* **18**(11), 117003 (2013).
13. Y. Zhou et al., "Calibration-free *in vivo* transverse blood flowmetry based on cross correlation of slow time profiles from photoacoustic microscopy," *Opt. Lett.* **38**(19), 3882–3885 (2013).
14. J. W. Tay, J. Y. Liang, and L. V. Wang, "Amplitude-masked photoacoustic wavefront shaping and application in flowmetry," *Opt. Lett.* **39**(19), 5499–5502 (2014).
15. R. M. Weight and J. A. Viator, "Detection of circulating tumor cells by photoacoustic flowmetry," in *Molecular Diagnostics for Melanoma: Methods and Protocols*, M. Thurin and F. Marincola, Eds., Vol. **1102**, pp. 655–663, Humana Press, New York (2014).
16. Y. Zhou et al., "*In vivo* photoacoustic flowmetry at depths of the diffusive regime based on saline injection," *J. Biomed. Opt.* **20**(8), 087001 (2015).
17. S. L. Chen et al., "Photoacoustic correlation spectroscopy and its application to low-speed flow measurement," *Opt. Lett.* **35**(8), 1200–1202 (2010).
18. S. L. Chen et al., "*In vivo* flow speed measurement of capillaries by photoacoustic correlation spectroscopy," *Opt. Lett.* **36**(20), 4017–4019 (2011).
19. R. Y. Zhang et al., "Structured-illumination photoacoustic Doppler flowmetry of axial flow in homogeneous scattering media," *Appl. Phys. Lett.* **103**(9), 094101 (2013).
20. J. Brunker and P. Beard, "Velocity measurements in whole blood using acoustic-resolution photoacoustic Doppler," *Biomed. Opt. Express* **7**(7), 2789–2806 (2016).
21. Y. Zhou, J. Y. Liang, and L.H.V. Wang, "Cuffing-based photoacoustic flowmetry in humans in the optical diffusive regime," *J. Biophotonics* **9**(3), 208–212 (2016).
22. R. Y. Zhang et al., "*In vivo* optically encoded photoacoustic flowgraphy," *Opt. Lett.* **39**(13), 3814–3817 (2014).
23. I. V. Larina, K. V. Larin, and R. O. Esenaliev, "Real-time optoacoustic monitoring of temperature in tissues," *J. Phys. D: Appl. Phys.* **38**(15), 2633–2639 (2005).
24. M. Pramanik and L. V. Wang, "Thermoacoustic and photoacoustic sensing of temperature," *J. Biomed. Opt.* **14**(5), 054024 (2009).
25. M. H. Xu and L.H.V. Wang, "Photoacoustic imaging in biomedicine," *Rev. Sci. Instrum.* **77**(4), 041101 (2006).
26. J. J. Yao et al., "High-speed label-free functional photoacoustic microscopy of mouse brain in action," *Nat. Methods* **12**(5), 407–410 (2015).
27. P. F. Hai et al., "Near-infrared optical-resolution photoacoustic microscopy," *Opt. Lett.* **39**(17), 5192–5195 (2014).
28. L. A. Sordillo et al., "Deep optical imaging of tissue using the second and third near-infrared spectral windows," *J. Biomed. Opt.* **19**(5), 056004 (2014).
29. P. X. Lai et al., "Photoacoustically guided wavefront shaping for enhanced optical focusing in scattering media," *Nat. Photonics* **9**(2), 126–132 (2015).
30. Y. M. Wang et al., "Deep-tissue focal fluorescence imaging with digitally time-reversed ultrasound-encoded light," *Nat. Commun.* **3**, 928 (2012).

Wei Liu is a postdoctoral associate in biomedical engineering at Duke University. He received his BE degree in optics in 2010 and PhD in physics in 2015 from Harbin Institute of Technology, China. Before joining the photoacoustic imaging group at Duke, he stayed at Nanyang Technological University, Singapore, as a research fellow. His current research interest focuses on photoacoustic imaging, biophotonics and biomedical instrumentation.

Bangxin Lan is a master's student in the Department of Biomedical Engineering at Duke University. His major research focus is in high-speed photoacoustic imaging.

Leo Hu is an undergraduate student at Duke University, currently pursuing both a BSE in biomedical engineering and a BSE in electrical and computer engineering. Currently, he is researching high-resolution photoacoustic imaging.

Ruimin Chen received his BS degree from University of Electronics Science and Technology of China, Chengdu, China, and his PhD from University of Southern California (USC), Los Angeles, California, in 2006 and 2014, respectively, both in biomedical engineering. Currently, he is a research associate in the NIH Resource Center for Medical Ultrasonic Transducer Technology of USC. His research interests include high-frequency ultrasonic transducers and arrays, piezoelectric material characterization, and photoacoustic imaging.

Qifa Zhou received his PhD from Xi'an Jiaotong University, Xi'an, China in 1993. Currently, he is a professor of ophthalmology, biomedical engineering at the University of Southern California. His research focuses on the development of piezoelectric high-frequency ultrasonic transducers for biomedical ultrasound and photoacoustic imaging, including intravascular imaging, cancer imaging, and ophthalmic imaging. He is also actively exploring ultrasonic mediated therapeutic technology including trans-sclera drug delivery, and ultrasound for retinal and brain stimulation.

Junjie Yao is an assistant professor of biomedical engineering at Duke University, and a faculty member of Duke Center for *In-Vivo* Microscopy and Fitzpatrick Institute for Photonics. He received his BE and ME degrees from Tsinghua University, and his PhD in biomedical engineering at Washington University, St. Louis. His research interest is in photoacoustic tomography technologies in life sciences, especially in functional brain imaging and early cancer detection.